Available online at www.sciencedirect.com
ScienceDirect
Catalysis Today 133–135 (2008) 611–618
CATALYSIS TODAY
www.elsevier.com/locate/cattod

Photocatalytic oxidation of cyanide on TiO_2: An electrochemical approach

J.A. Pedraza-Avella [a], P. Acevedo-Peña [b], J.E. Pedraza-Rosas [b,*]

[a] *Centro de Investigaciones en Catálisis – CICAT, Universidad Industrial de Santander – UIS, Sede Guatiguará, Km. 2 vía El Refugio, Piedecuesta (Santander), Colombia*
[b] *Grupo de Investigaciones en Minerales, Biohidrometalurgia y Ambiente – GIMBA, Universidad Industrial de Santander – UIS, Sede Guatiguará, Km. 2 vía El Refugio, Piedecuesta (Santander), Colombia*

Available online 4 March 2008

Abstract

Photocatalytic oxidation of cyanide on TiO_2 was studied by means of voltammetry, linear polarization resistance and Tafel polarization using TiO_2–carbon paste electrodes (TiO_2–CPEs). In all cases, a positive effect with UV–vis illumination on the oxidation current (i.e. oxidation rate) was observed, showing the convenience of this type of electrodes for the electrochemical evaluation of powdered semiconductor photocatalysts. Voltammetric results indicated that the oxidation of cyanide (CN^-) occurs at lower potentials than the oxidation of hydroxyl ions (OH^-); cyanide is oxidized to cyanate (CNO^-) and at high potentials it can further be oxidized together with OH^-. Linear polarization resistance curves showed that the process is controlled by electron transfer. Tafel slopes from the anodic and cathodic polarization curves enabled the determination of the intrinsic kinetic parameters of the reaction (i.e. rate constant, reaction orders). UV–vis illumination led to an increase in the reaction rate, related to the increment in the rate constant, and a decrease in the reaction orders for both CN^- and OH^- ions.

Keywords: Heterogeneous photocatalysis; Titanium dioxide; Carbon paste electrodes; Cyanide; Electrochemical techniques

1. Introduction

Heterogeneous photocatalysis is an emerging technology for water treatment that allows the pollutants elimination even at very low concentrations. It is based on the surface reactions that occur on a photoexcited semiconductor [1,2].

Titanium dioxide has been the most used photocatalyst due to its optical and electronic properties, chemical stability, non-toxicity and low cost. TiO_2 is an *n*-type semiconductor which exists in two main crystallographic forms, anatase and rutile. In most cases, anatase has been found to be more photocatalytically active than rutile [2,3].

Photocatalytic oxidation of cyanide (CN^-) has been the object of several works, due to its high toxicity [4–15]. It has been found that cyanate (CNO^-) is its principal oxidation product and under certain conditions this ion can further be photocatalytically oxidized on TiO_2 forming less toxic products such as carbonate (CO_3^{2-}), nitrite (NO_2^-), nitrate (NO_3^-), carbon dioxide (CO_2) and nitrogen (N_2) [5–9,15]. It is still debatable whether the photocatalytic oxidation of cyanide by TiO_2 particles in suspension proceeds via photoholes (a pure heterogeneous pathway) or via photogenerated hydroxyl radicals (an indirect pathway mediated by adsorbed hydroxyl radicals or a homogeneous pathway by diffused hydroxyl radicals) [13,14].

Furthermore, it is important to highlight the growing interest in understanding photocatalytic reactions using electrochemical techniques, due to the nature of the redox processes involved therein [16–21]. These techniques allow *in situ* and *operando* studies of the photocatalysts in working electrodes and a complete evaluation of the reactions taking place, offering thermodynamic and intrinsic kinetic information in a simple, rapid and accurate manner.

Relevant parameters in photocatalytic experimentation such as mass of photocatalyst, radiant flux and concentration of reactants can be precisely controlled in an electrochemical evaluation by keeping constant the area and the composition of

* Corresponding author. Tel.: +57 7 6550802; fax: +57 7 6550802.
E-mail addresses: apedraza@uis.edu.co (J.A. Pedraza-Avella), jpedraza@uis.edu.co (J.E. Pedraza-Rosas).

0920-5861/$ – see front matter © 2008 Elsevier B.V. All rights reserved.
doi:10.1016/j.cattod.2007.12.063

the electrode, as well as a small ratio between the electrode area and the electrolyte volume so that the passage of current does not alter the bulk concentrations of electroactive species [21,22].

It is worth mentioning that electrochemical techniques enable an independent study of the two half-reactions, oxidation (anodic) and reduction (cathodic), which usually occur on the photocatalyst because they will take place in different electrodes. In addition, the application of a potential bias can be used to suppress the electron–hole recombination and then manipulate the rate-determining step of the overall photocatalytic process (i.e. mass transfer or electron transfer). This overcomes the interference of electron removal by oxygen, an important aspect in slurry systems in which kinetics of the photocatalytic process is often controlled by such half-reaction (reduction of O_2) [21].

Additionally, with an electrochemical approach, the current resulted from the photocatalytic oxidation can be readily measured and employed to determine the instantaneous rate of reaction, which directly reflects the photocatalytic efficiency of the system regardless of the type of compounds and their oxidation degree [18,21]. This contrasts with the conventional kinetic study method in which the rate of reactant disappearance is usually employed to express the photocatalytic reaction rate [23].

The application of electrochemical techniques requires the preparation of working electrodes with the photocatalysts. For this purpose, TiO_2 single crystals [16], anodization of titanium sheets [17], TiO_2 films on conducting glass slides [18,20,21] and thermal decomposition of $TiCl_4$ on titanium plates [19] have been employed.

Although carbon paste electrodes (CPEs) have shown their convenience in the electrochemical study of powdered minerals (e.g. chalcopyrite, galena and pyrite: *n*-type semiconductors) and they can be prepared by a simple, rapid, inexpensive and reliable method [24–26], to our knowledge, CPEs have not been used in the evaluation of photocatalysts.

CPEs can be made of fine particles of photocatalyst mixed with graphite and a binding material, which may be or not electroactive. Non-conducting binders such as organic or mineral oils usually are hydrophobic and therefore they only allow that the electrochemical reactions take place at the electrode–electrolyte interface. In addition, CPEs enable a simple renovation of the electrode surface for each new experiment, thus providing precise and accurate results [27].

Recently, it has been reported that the modification of TiO_2 electrodes with a suitable carbon powder allows them to be used in solar cells with improved performance and minor side effects [28].

This work constitutes an initial approach to study the photocatalytic oxidation of cyanide on TiO_2 by means of electrochemical techniques (voltammetry, linear polarization resistance and Tafel polarization) using TiO_2–carbon paste electrodes (TiO_2–CPEs). The obtained results allowed the determination of some aspects of the electrochemical mechanism and the intrinsic kinetic parameters of reaction.

2. Thermodynamic considerations

When a semiconductor photocatalyst such as TiO_2 is illuminated with photons whose energy is equal to or higher than their band-gap energy (E_g = 3.23 eV for anatase), there is absorption of these photons and generation within the bulk of electron–hole pairs. These electron–hole pairs dissociate into free photoelectrons in the conduction band e^-_{CB} and photoholes in the valence band h^+_{VB} as shown in Eq. (1).

$$TiO_2 \xrightarrow[(\lambda \leq 384\,nm)]{h\nu\,UV} TiO_2^* \equiv \{e^-_{CB} \cdots h^+_{VB}\} \quad (1)$$

Some of the photoelectrons and photoholes, those that do not undergo recombination, can get to the surface of the photocatalyst and then an electron transfer proceeds towards adsorbed acceptor molecules A (Eq. (2)), whereas positive photoholes are transferred to adsorbed donor molecules D (Eq. (3)). The photohole transfer corresponds to the cession of an electron by donor molecules to the photocatalyst.

$$A_{(ads)} + e^-_{CB} \rightarrow A^{\bullet -}_{(ads)} \quad (2)$$

$$D_{(ads)} + h^+_{VB} \rightarrow D^{\bullet +}_{(ads)} \quad (3)$$

From a thermodynamic point of view, a chemical species A can be photocatalytically reduced by e^-_{CB} only if the conduction band potential of the photocatalyst is more negative than the redox potential of the species A. In the same way, a chemical species D can be photocatalytically oxidized by h^+_{VB} only if the valence band potential of the photocatalyst is more positive than the redox potential of the species D. Both reactions should occur simultaneously because electroneutrality has to be maintained [2,3].

It is important to point out that the potentials of both conduction and valence bands of TiO_2 follow a Nernstian pH dependence, decreasing 59 mV per pH unit according to Eqs. (4) and (5), and consequently, the ability of electrons and holes to participate in redox processes is determined by the pH of the medium [29]. The values of the standard redox potentials cited here are expressed in *V* and referred to the normal hydrogen electrode (NHE), unless otherwise indicated.

$$E_{CB} = -0.05 - 0.059\,pH \quad (\text{anatase at } 25\,^\circ C) \quad (4)$$

$$E_{VB} = 3.15 - 0.059\,pH \quad (\text{anatase at } 25\,^\circ C) \quad (5)$$

If this behavior is represented in a potential vs. pH diagram (Pourbaix diagram) together with the electrochemical behavior of the species from a particular system in aqueous solution, it can be used to establish what photocatalytic reactions are spontaneous and to predict possible oxidation–reduction products as function of the pH [30].

The Pourbaix diagram for the H_2O–CN^- system obtained with HSC Chemistry 4.1 software (Outokumpu Research Oy, Finland), which also contains the positions of conduction and valence bands of TiO_2 anatase, is shown in Fig. 1. Gray dashed lines represent the stability field of water, black solid lines

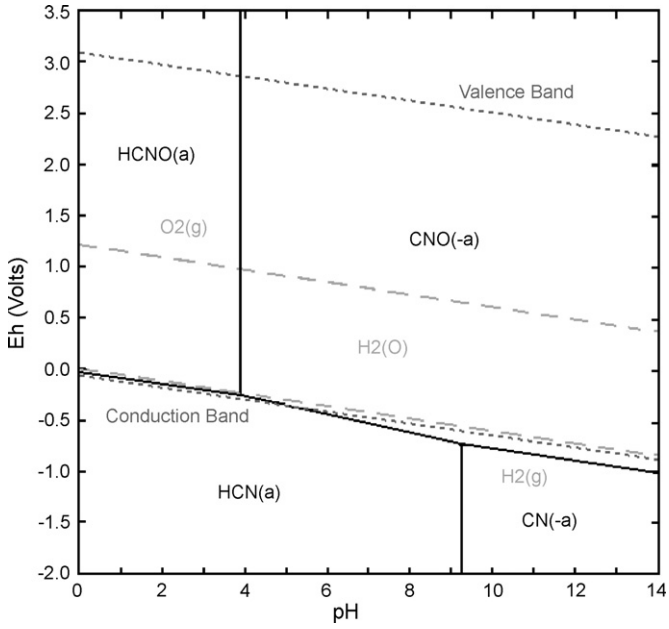

Fig. 1. Pourbaix diagram for the H_2O–CN^- system with the potentials of conduction and valence bands of TiO_2 anatase. CN^-, HCN, $(CN)_2$, CNO^- and HCNO species were considered.

indicate the stability regions of the chemical species, and black dotted lines indicate the potentials of TiO_2 bands.

Keeping in mind that the oxidation of CN^- occurs through the formation of cyano radical ($CN^{\bullet}$) according to Eqs. (6)–(9) [13,31], cyanogen ($(CN)_2$) was also used for making the Pourbaix diagram as an input data in the software. However, this species not appears in Fig. 1 because it is not thermodynamically stable in water.

$$CN^-_{(ads)} + h^+_{VB} \rightarrow CN^{\bullet}_{(ads)} \quad (6)$$

$$CN^{\bullet}_{(ads)} + 2OH^- + h^+_{VB} \rightarrow CNO^- + H_2O \quad (7)$$

$$2CN^{\bullet}_{(ads)} \rightarrow (CN)_2 \quad (8)$$

$$(CN)_2 + 2OH^- \rightarrow CNO^- + CN^- + H_2O \quad (9)$$

It can also be observed from Fig. 1 that the oxidation of CN^- to produce CNO^- is thermodynamically allowed through a photocatalytic pathway on TiO_2 as well as the reduction of O_2 and H_2O. The formation of toxic hydrogen cyanide (HCN) should be avoided by keeping a pH > 9.3. Cyanic acid (HCNO) would be formed at pH < 4.

From an electrochemical point of view, the photocatalytic oxidation of CN^- on TiO_2 in the presence of O_2 as electron scavenger can be described through the following reactions of electron transfer (Eqs. (10) and (11)) [32,33], which are in concordance with those reported in the literature [4–10,13]:

$$CN^- + 2OH^- + 2h^+_{BV} \rightarrow CNO^- + H_2O \quad E = -0.144 - 0.059\,pH \quad (at\ 25\,^{\circ}C) \quad (10)$$

$$^1/_2O_2 + H_2O + 2e^-_{BC} \rightarrow 2OH^- \quad E = 1.229 - 0.059\,pH \quad (at\ 25\,^{\circ}C) \quad (11)$$

3. Experimental

3.1. Materials

The following reagents were used as received without additional purification: TiO_2 (Merck, 99.5%) was used as photocatalyst. Graphite powder (Aldrich, 99.99%, −100 mesh) and mineral oil (Aldrich, light) were employed in the preparation of the carbon paste electrodes. NaCN (Aldrich, 97%), NaOH pellets (J.T. Baker, 98.5%), distilled water ($\rho > 1\ M\Omega$ cm) and compressed nitrogen (Praxair, 99.999%) were used in the electrochemical evaluation of the photocatalytic oxidation of cyanide. NaCl (Merck, 99.5%) was employed as support electrolyte.

3.2. Characterization of the photocatalyst

Crystal phase composition of the photocatalyst was determined by powder X-ray diffraction (XRD) at room temperature using a Rigaku D/MAX-IIIB diffractometer with Cu Kα radiation. Crystallite size of the photocatalyst was estimated from the diffraction peak (1 0 1) by applying the Scherrer equation [34].

Specific surface area of the photocatalyst was determined by N_2 adsorption at liquid-nitrogen temperature with a Quantachrome NOVA 1200 apparatus using the multipoint Brunauer–Emmett–Teller (BET) method. Total pore volume and average pore diameter of the photocatalyst was obtained from the adsorption/desorption isotherm using the Barrett–Joyner–Halenda (BJH) method [35].

The isoelectric point (IEP) of the photocatalyst was determined by zeta (ζ) potential measurements at different pH values using a Zeta-Meter 3.0+ apparatus [34].

The band-gap energy of the photocatalyst was estimated by UV–vis diffuse reflectance spectroscopy (DRS) with a PerkinElmer Lambda 4B spectrometer. MgO was used as reference (100% reflectance sample) [35].

3.3. Preparation of the electrodes

TiO_2–CPEs were prepared according to the procedure described by Cisneros-González et al. [25] for the electrochemical evaluation of minerals, using a TiO_2:graphite weight ratio of 70:30. The geometric area of the electrode was 0.03 cm^2.

3.4. Photoelectrochemical tests

TiO_2–CPEs were tested using the electrochemical techniques of cyclic and linear sweep voltammetry, linear polarization resistance and Tafel polarization measurements.

Voltammetry tests were made with a Pine AFCBP1 computer-controlled bipotentiostat. Linear polarization resistance and Tafel polarization measurements were made with a Gamry PC4/750 potentiostat/galvanostat/ZRA.

All experiments were carried out in a standard three-electrode cell constructed from a modified 250 mL flask of Pyrex glass (Ace Glass 6961-70) with flat bottom to avoid

radiation dispersion. TiO_2–CPE was used as working electrode, a Pt wire as counter electrode and an Ag/AgCl (3 M) electrode as reference.

All solutions were deoxygenated by bubbling nitrogen 10 min prior to each experiment. During the experiments, the nitrogen flow was maintained at the solution surface to get an inert atmosphere.

Electrochemical tests were carried out in the dark and with UV–vis illumination, provided by a high-pressure mercury lamp (General Electric, Kolorlux 125 W) placed below the cell. The working electrode surface was fully illuminated from the bottom of the cell. The emission spectrum of the lamp was recorded photographically on a Kodak film (ASA 400) with a Jarrell-Ash 3.4 m Ebert spectrograph. The radiant flux entering the electrochemical cell was measured with a Newport 1815-C optical power meter equipped with an 818-UV silicon detector (190–1100 nm).

The experiments were accomplished about 10 min after immersing the electrodes in about 175 mL of the assay solution, in order to get the adsorption of reactants, the lamp stabilization and in some cases the open-circuit potential.

4. Results and discussion

4.1. Characterization of the photocatalyst

The results of the photocatalyst characterization are summarized in Table 1.

Further studies with the TiO_2–graphite mixture would be useful for the estimation of the graphite effect in the photophysical (light absorption, band-gap energy, flat-band potentials) and textural (specific surface area, porosity) properties of the photocatalyst.

4.2. Photoelectrochemical tests

The lamp used in the photoelectrochemical tests provides maximum energy at 365 nm with substantial radiation also at 313, 334, 404, 435, 546 and 578 nm. Pyrex glass cut off wavelengths below 310 nm. The incident radiant flux was about 45 mW/cm^2.

4.2.1. Voltammetry

Cyclic voltammetry was used to study the electrochemical behaviors of a pure carbon paste electrode (100% graphite) in 100 ppm NaCN solution and TiO_2–CPE in distilled water (using 0.25 M NaCl as support electrolyte), in the dark and with UV–vis illumination.

Although it was found that the electrochemical oxidation of cyanide can take place on a pure carbon paste electrode in the dark, it is worth noting that it did not show any improvement with UV–vis light. Furthermore, the photocatalytic oxidation of graphite or mineral oil by TiO_2 can be discarded from −1000 to 1000 mV vs. Ag/AgCl because non-anodic currents were detected at this potential range during the voltammetric evaluation of TiO_2–CPE in distilled water (using 0.25 M NaCl as support electrolyte) with UV–vis illumination.

Since aqueous cyanide solutions are only stable in alkaline media (see Fig. 1), the oxidation of OH^- (Eq. (12)) could simultaneously occur with the oxidation of CN^- (Eq. (10)) competing for h^+_{VB} of the photocatalyst.

$$2OH^-_{(ads)} + 2h^+_{VB} \rightarrow {}^1/_2O_2 + H_2O \quad (12)$$

Taking into account one-electron transfer steps, the oxidation of OH^- (Eq. (12)) involves the formation of oxidant species such as hydroxyl radical ($OH^\bullet$), monoatomic oxygen ($O^\bullet$) and hydrogen peroxide (H_2O_2), according to Eqs. (13)–(18) [36].

$$OH^-_{(ads)} + h^+_{VB} \rightarrow OH^\bullet_{(ads)} \quad (13)$$

$$OH^\bullet_{(ads)} + OH^- + h^+_{VB} \rightarrow O^\bullet + H_2O \quad (14)$$

$$OH^\bullet_{(ads)} \rightarrow OH^\bullet \quad (15)$$

$$2OH^\bullet \rightarrow H_2O_2 \quad (16)$$

$$H_2O_2 \rightarrow O^\bullet + H_2O \quad (17)$$

$$2O^\bullet \rightarrow O_2 \quad (18)$$

In order to study the electrochemical behavior of OH^- on TiO_2–CPE, cyclic voltammograms were taken in a 200 mM NaOH solution (using 0.25 M NaCl as support electrolyte), in the dark and with UV–vis illumination, at a scan rate of 20 mV/s. The resulting curves are shown in Fig. 2.

An enhancement in the current with the illumination is clearly observed in Fig. 2 during the potential scan. It is worth noting that cathodic currents appear at the beginning of the scan. Anodic currents due to the oxidation of OH^- appear in the potential range from 0 to 1000 mV vs. Ag/AgCl.

Linear sweep voltammetry was used to study the effect of CN^- concentration in the NaOH solution. Voltammograms obtained in 200 mM NaOH solutions with different NaCN concentrations (0, 100 and 1000 ppm), in the dark and with UV–vis illumination, at a scan rate of 20 mV/s are shown in Fig. 3.

Table 1
TiO_2 characterization

XRD			N_2 adsorption			ζ Potential	UV–vis DRS	
Anatase (wt.%)	Rutile (wt.%)	Crystallite size (nm)	Specific surface area (m^2/g)	Total pore volume ($cm^3/g \times 10^3$)	Average pore diameter (Å)	IEP	λ (nm)	E_g (eV)
97.5	2.5	53	8.9	25.8	57.8	3.7	387	3.21

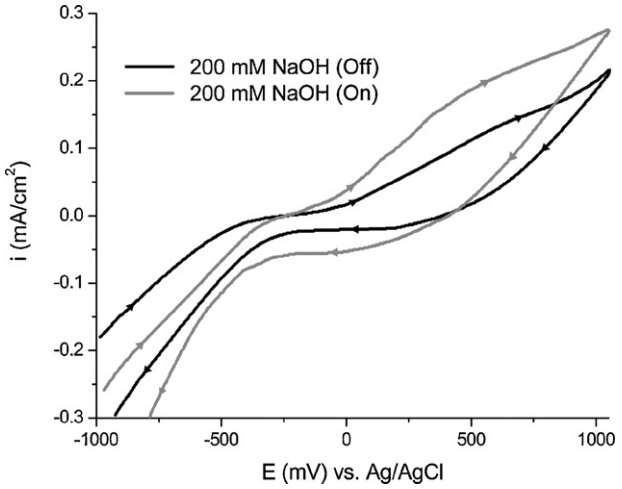

Fig. 2. Cyclic voltammograms in a 200 mM NaOH solution, in the dark (black line) and with UV–vis illumination (gray line), at a scan rate of 20 mV/s.

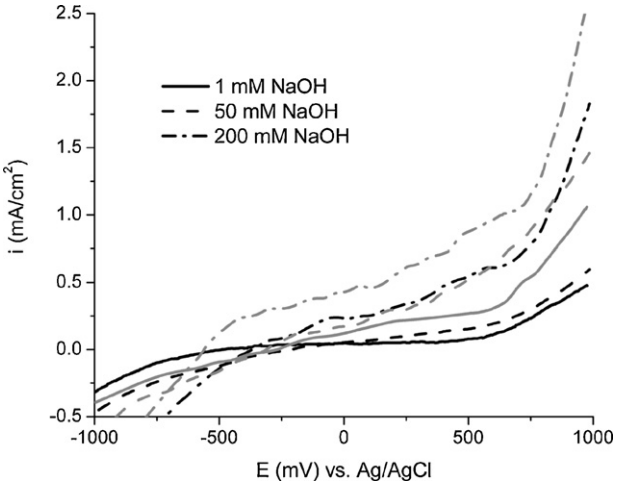

Fig. 4. Linear sweep voltammograms in 1000 ppm NaCN solutions with different NaOH concentrations, in the dark (black lines) and with UV–vis illumination (gray lines), at a scan rate of 20 mV/s.

The positive effect of the illumination is also observed in Fig. 3, as well as a significant effect of the CN^- concentration in the shape of the curves. With the increase of CN^- concentration, anodic currents at more negative potentials appear and increase along the potential range. This is attributed to the oxidation of CN^- (Eq. (10)), which takes place in the potential range from −500 to 0 mV vs. Ag/AgCl, below the potential range corresponding to oxidation of OH^-. These results indicate that the oxidation of CN^- by photoholes is thermodynamically more favorable than the oxidation of OH^- (i.e. generation of $OH^\bullet$), and they are in agreement with the Pourbaix diagram (see Fig. 1).

An increment in the currents at the end of the scan, in the potential range from 750 to 1000 mV vs. Ag/AgCl, was registered when cyanide concentration increased. This was especially remarkable at 1000 ppm NaCN.

In order to investigate if this effect is due to the oxidation of OH^- or can be attributed to the oxidation of CNO^- (i.e. the advanced oxidation of CN^-), another series of linear sweep voltammograms were recorded in 1000 ppm NaCN solutions with different NaOH concentrations (1, 50 and 200 mM) in the dark and with UV–vis illumination at a scan rate of 20 mV/s, as are shown in Fig. 4.

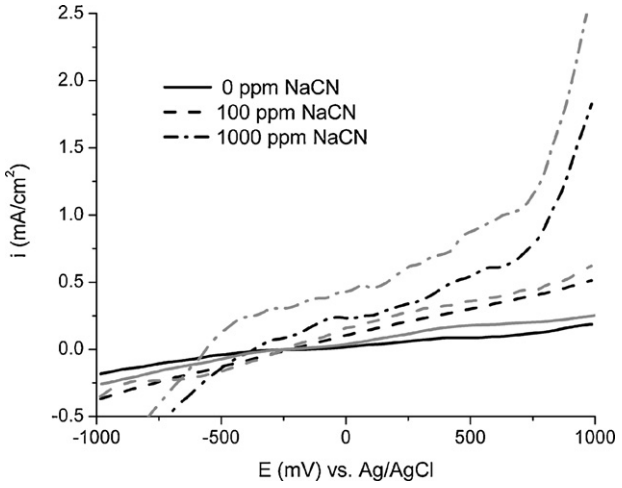

Fig. 3. Linear sweep voltammograms in 200 mM NaOH solutions with different NaCN concentrations, in the dark (black lines) and with UV–vis illumination (gray lines), at a scan rate of 20 mV/s.

In Fig. 4, besides the positive effect of the illumination, a significant increase in the current at the end of the scan and curves with nearly the same shape was registered in all cases. Is worth noting that this increment is slightly more marked when OH^- concentration increases. These results suggest that at high potentials the oxidation of CNO^- may occur together with the oxidation of OH^-.

It is important to point out that the oxidation of CNO^- as well as the oxidation of OH^- should take place at the electrode surface according to the detected currents. The thermodynamic feasibility for the photocatalytic oxidation of CNO^- on TiO_2 is suggested by Fig. 1 which indicates the high oxidation potential of the valence band. Other chemical reactions of non-electrochemical nature or in homogeneous phase such as the hydrolysis of cyanate [37] also could be occurring but they cannot be directly detected by electrochemical techniques.

Although the voltammetric study contains sufficient information to sustain these conclusions, voltammetric measurements using synthetic solutions of $(CN)_2$ and CNO^- would be useful to confirm the species participating on the mechanism [31].

4.2.2. Linear polarization resistance

These experiments were carried out at the open-circuit potential (E_{oc}) of the working electrode. The corresponding E_{oc} values of TiO_2–CPE in all solutions studied, measured in the dark and with UV–vis illumination, are reported in Table 2.

UV–vis illumination as well as the increase of CN^- or OH^- concentrations implies a decrease in the E_{oc} value, which is attributed to a depolarization of the anodic reactions (oxidations) that take place spontaneously on the electrode.

The linear polarization resistance curves obtained for TiO_2–CPE in solutions with CN^- and OH^- concentrations in the

Table 2
TiO_2–CPE open-circuit potentials as a function of CN^- and OH^- concentrations, in the dark and with UV–vis illumination

[NaCN] (ppm)	[NaOH] (mM)	E_{oc} (mV vs. Ag/AgCl)	
		Off	On
0	200	55	50
100	200	−95	−132
500	200	−173	−180
1000	200	−184	−198
1000	50	−79	−106
1000	1	231	−18

studied range showed a lineal behavior which evidences that the process was controlled by electron transfer [38]. Curves obtained for 200 mM NaOH solution with the lower CN^- concentration (100 ppm NaCN), in the dark and with UV–vis illumination, at a scan rate of 0.125 mV/s are shown in Fig. 5.

The fact that the measurements were made 10 min after immersing the electrodes (pre-adsorption time) and the beneficial effect of carbon for cyanide adsorption [31], as well as the short times of electrochemical evaluation and the application of a potential bias, enabled that the process was controlled by electron transfer. This contrasts with the conventional photocatalytic oxidation of cyanide using TiO_2 in suspension, in which the low adsorption of cyanide ions onto the titanium dioxide surface limits the reaction [13].

In order to determine mass transfer limitations and to study adsorbed species phenomena, additional experiments could be carried out with and without stirring, and in presence and absence of surfactants [31].

4.2.3. Tafel polarization

This technique allows the evaluation of the reactions that occur on the working electrode when operating near to its E_{oc} and enables to determine the effect of different variables on the total oxidation current (i.e. oxidation rate). This is a great advantage because the intrinsic kinetic parameters of the reaction (i.e. rate constants, reaction orders) can be estimated [39], particularly when the process is controlled by electron transfer such as in the present study.

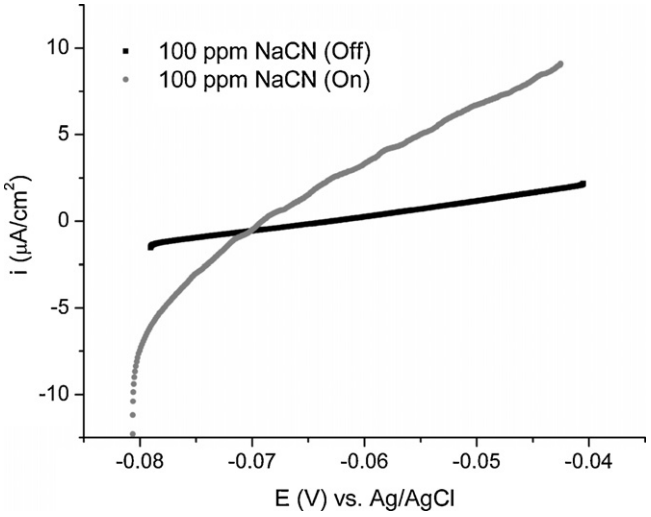

Fig. 5. Linear polarization resistance curves in a 100 ppm NaCN and 200 mM NaOH solution, in the dark (black dots) and with UV–vis illumination (gray dots), at a scan rate of 0.125 mV/s.

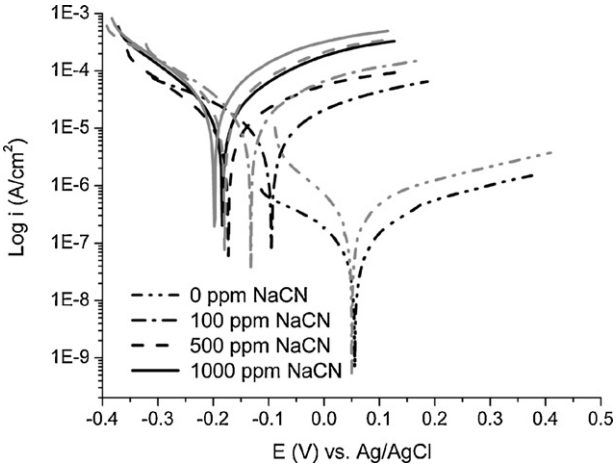

Fig. 6. Tafel polarization curves in 200 mM NaOH solutions with different NaCN concentrations, in the dark (black lines) and with UV–vis illumination (gray lines), at a scan rate of 0.125 mV/s.

Tafel polarization curves recorded for TiO_2–CPE in solutions with different CN^- and OH^- concentrations, in the dark and with UV–vis illumination, at a scan rate of 0.125 mV/s are shown in Figs. 6 and 7, respectively.

In all cases, illumination led to a current increase moving up the curves and also displacing them to a lower potential range. The increase in CN^- and OH^- concentrations also gives a similar effect, showing that the obtained currents are a function of these variables.

In Fig. 6, it is important to point out that a low CN^- concentration (100 ppm NaCN) yields a curve displacement toward higher current values. Higher increments in CN^- concentration do not result in such a remarkable increase in the currents.

In Fig. 7, a stronger influence of the illumination on the current was observed at low OH^- concentration (1 mm NaOH).

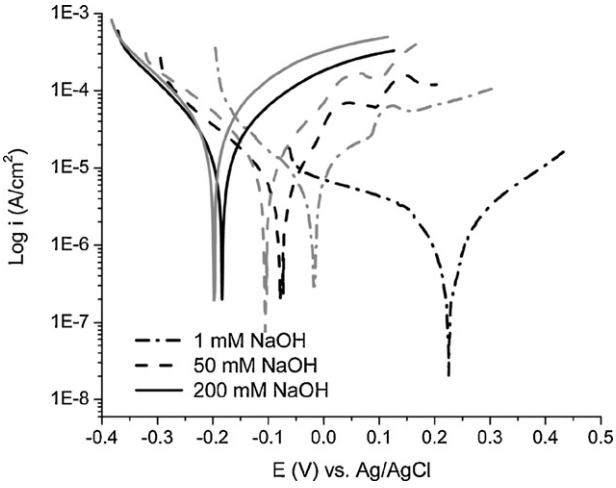

Fig. 7. Tafel polarization curves in 1000 ppm NaCN solutions with different NaOH concentrations, in the dark (black lines) and with UV–vis illumination (gray lines), at a scan rate of 0.125 mV/s.

Table 3
Oxidation current density referred to CN^- and OH^- concentrations, in the dark and with UV–vis illumination

Concentration	i_{ox} (A/cm^2)	
	Off	On
[CN^-] (mM)		
0	4.56×10^{-8}	2.04×10^{-7}
0.51	2.66×10^{-6}	9.07×10^{-6}
2.55	6.00×10^{-6}	1.32×10^{-5}
5.10	1.18×10^{-5}	1.42×10^{-5}
[OH^-] (mM)		
1	7.28×10^{-7}	2.72×10^{-6}
50	5.14×10^{-6}	7.04×10^{-6}
200	1.18×10^{-5}	1.42×10^{-5}

The values of oxidation current density (i_{ox}) in the dark and with UV–vis illumination were obtained by the Tafel extrapolation method from Figs. 6 and 7 and they are summarized in Table 3. The slopes were estimated in the well-defined lineal regions at about 50 mV from E_{oc} for both cathodic and anodic branches (over at least one decade of current) [39].

Since the Tafel test was carried out in the absence of O_2 and near to E_{oc}, at a lower potential than the range where oxidation of OH^- or CNO^- acquires importance, the overall electrochemical process only involves the oxidation of CN^- (Eq. (10)) and the reduction of H_2O in alkaline media (Eq. (19)), which can occur spontaneously on TiO_2 (see Fig. 1).

$$2H_2O + 2e^- \rightarrow H_2 + 2OH^- \qquad E = 0.000 - 0.059\,pH \quad (at\,25\,^\circ C) \tag{19}$$

Therefore, the intrinsic kinetics of the process can be described by the following expression (Eq. (20)):

$$r = k[CN^-]^n[OH^-]^m[H_2O]^k \tag{20}$$

Since CN^- and OH^- concentrations were independently varied and H_2O concentration can be considered constant, the intrinsic kinetics for the oxidation of CN^- can be expressed by the following equations (Eqs. (21) and (22)):

$$r = k_1[CN^-]^n \tag{21}$$

$$r = k_2[OH^-]^m \tag{22}$$

Keeping in mind the proportionality between i_{ox} and oxidation rate (r), the graphs ln r vs. ln [CN^-] and ln r vs. ln [OH^-] were constructed. The values for rate constant and reaction orders were calculated by lineal regression, as shown in Table 4 together with the obtained correlation coefficients (R^2).

It can be observed from Table 4 that the presence of UV–vis light yields an increase in the rate constant and a decrease in the reaction orders for both CN^- and OH^- concentrations. UV–vis illumination always enhanced the reaction rate and made it less dependent on the bulk concentrations of the reactive species.

It is worth mentioning that the low dependence of the oxidation rate on the concentration of the pollutants is a great advantage for heterogeneous photocatalysis over conventional techniques of water treatment, which are usually effective only at high concentrations of pollutants.

Table 4
Tafel kinetic parameters

Species	Illumination	Constant	Order	R^2
CN^-	Off	3.88×10^{-6}	0.62	0.97
	On	1.05×10^{-5}	0.20	0.98
OH^-	Off	7.16×10^{-7}	0.52	0.99
	On	2.61×10^{-6}	0.30	0.98

5. Conclusions

Carbon paste electrodes are appropriate for the electrochemical evaluation of powdered semiconductors in photocatalytic reactions.

The voltammetric evaluation indicated in terms of the electrochemical potential that the oxidation of OH^- occurs after the oxidation of CN^- and slightly before the oxidation of CNO^-.

In the absence of mass transfer limitations, such as in the present study where this was demonstrated by the linear polarization resistance curves, the oxidation of CN^- proceeds via photoholes preferably than via photogenerated hydroxyl radicals.

The Tafel slopes from the polarization curves showed that UV–vis illumination enhanced the reaction rate and made it less dependent on the bulk concentrations of reactive species, because it implies an increase in the intrinsic rate constant and a decrease in the reaction orders for both CN^- and OH^- ions.

Acknowledgements

This work has been carried out with the financial support of UIS (DIEF Ciencias, Proyecto 5125). J.A. Pedraza-Avella thanks COLCIENCIAS for the doctoral scholarship in the frame of the program ''Apoyo a la Comunidad Científica Nacional, a través de los Programas de Doctorados Nacionales, 2003''. The authors would like to thank C. Vásquez (Grupo de Investigaciones en Corrosión, UIS, Escuela de Ingeniería Metalúrgica y Ciencia de los Materiales) and especially I. González (Universidad Autónoma Metropolitana-Iztapalapa, Departamento de Química, Área de Electroquímica, México D.F.) for their very helpful comments, suggestions, improvements and corrections.

References

[1] J. Blanco, S. Malato, C.A. Estrada Gasca, E.R. Bandala, S. Gelover, T. Leal, In: M.A. Blesa, B. Sánchez (Eds.), Eliminación de Contaminantes por Fotocatálisis Heterogénea, CIEMAT, Madrid, 2004, p. 67.
[2] J.-M. Herrmann, Top. Catal. 34 (2005) 49.
[3] M.I. Litter, Appl. Catal. B: Environ. 23 (1999) 89.
[4] S.N. Frank, A.J. Bard, J. Am. Chem. Soc. 99 (1977) 303.
[5] J. Peral, J. Muñoz, X. Domènech, J. Photochem. Photobiol. A: Chem. 55 (1990) 251.

[6] Cy.H. Pollema, J.L. Hendrix, E.B. Milosavljević, L. Solujić, J.H. Nelson, J. Photochem. Photobiol. A: Chem. 66 (1992) 235.
[7] H. Hidaka, T. Nakamura, A. Ishizaka, M. Tsuchiya, J. Zhao, J. Photochem. Photobiol. A: Chem. 66 (1992) 367.
[8] V. Augugliaro, V. Loddo, G. Marcì, L. Palmisano, M.J. López-Muñoz, J. Catal. 166 (1997) 272.
[9] V. Augugliaro, J. Blanco Gálvez, J. Cáceres Vázquez, E. García López, V. Loddo, M.J. López Muñoz, S. Malato Rodríguez, G. Marcì, L. Palmisano, M. Schiavello, J. Soria Ruiz, Catal. Today 54 (1999) 245.
[10] S.P. Hudson, M. Shirkhanzadeh, C.A. Pickles, Miner. Process. Extr. Metall. 109 (2000) 137.
[11] B. Dąbrowski, A. Zaleska, M. Janczarek, J. Hupka, J.D. Miller, J. Photochem. Photobiol. A: Chem. 151 (2002) 201.
[12] J. Aguado, R. van Grieken, M.J. López-Muñoz, J. Marugán, Catal. Today 75 (2002) 95.
[13] K. Chiang, R. Amal, T. Tran, J. Mol. Catal. A: Chem. 193 (2003) 285.
[14] J.-H. Kim, H.-I. Lee, Korean J. Chem. Eng. 21 (2004) 116.
[15] A. Bozzi, I. Guasaquillo, J. Kiwi, Appl. Catal. B: Environ. 51 (2004) 203.
[16] K. Kogo, H. Yoneyama, H. Tamura, J. Phys. Chem. 84 (1980) 1705.
[17] B.-J. Hwang, S.-S. Jeng, J. Chin. Inst. Chem. Eng. 24 (1993) 401.
[18] J.M. Kesselman, N.S. Lewis, M.R. Hoffmann, Environ. Sci. Technol. 31 (1997) 2298.
[19] R. Pelegrini, P. Peralta-Zamora, A.R. de Andrade, J. Reyes, N. Durán, Appl. Catal. B: Environ. 22 (1999) 83.
[20] T. Lana-Villarreal, R. Gómez, Electrochem. Commun. 7 (2005) 1218.
[21] D. Jiang, H. Zhao, S. Zhang, R. John, J. Photochem. Photobiol. A: Chem. 177 (2006) 253.
[22] A.J. Bard, L.R. Faulkner, Electrochemical Methods: Fundamentals and Applications, second ed., Wiley, New York, 2001, p. 156.
[23] J.F. Walling, J. Chem. Educ. 45 (1968) 109.
[24] I. Lázaro, N. Martínez-Medina, I. Rodríguez, E. Arce, I. González, Hydrometallurgy 38 (1995) 277.
[25] I. Cisneros-González, M.T. Oropeza-Guzmán, I. González, Electrochim. Acta 45 (2000) 2729.
[26] C.M.V.B. Almeida, B.F. Giannetti, Electrochem. Commun. 4 (2002) 985.
[27] J.L. Nava, I. González, Quim. Nova 28 (2005) 901.
[28] S.H. Kang, J.-Y. Kim, Y.-K. Kim, Y.-E. Sung, J. Photochem. Photobiol. A: Chem. 186 (2007) 234.
[29] D. Chen, A.K. Ray, Chem. Eng. Sci. 56 (2001) 1561.
[30] M. Pourbaix, Atlas of Electrochemical Equilibria in Aqueous Solutions, Pergamon, Oxford, 1966, p. 29.
[31] V. Reyes-Cruz, I. González, M.T. Oropeza, J. Solid State Electrochem. 9 (2005) 566.
[32] G. Milazzo, S. Caroli, V.K. Sharma, Tables of Standard Electrode Potentials, Wiley, New York, 1978, p. 147, 229.
[33] A.J. Bard, R. Parsons, J. Jordan (Eds.), Standard Potentials in Aqueous Solution, Marcel Dekker, New York, 1985, p. 54, 199.
[34] X.Z. Li, F.B. Li, Environ. Sci. Technol. 35 (2001) 2381.
[35] T. López, J. Hernández-Ventura, R. Gómez, F. Tzompantzi, E. Sánchez, X. Bokhimi, A. García, J. Mol. Catal. A: Chem. 167 (2001) 101.
[36] O. Legrini, E. Oliveros, A.M. Braun, Chem. Rev. 93 (1993) 671.
[37] A. Bravo, J. Garcia, X. Doménech, J. Peral, Electrochim. Acta 39 (1994) 2461.
[38] R.G. Nelly, J.R. Scully, D.W. Shoesmith, R.G. Buchheit, Electrochemical Techniques in Corrosion Science and Engineering, Marcel Dekker, New York, 2003, p. 125.
[39] E. McCafferty, Corros. Sci. 47 (2005) 3202.